ISSN: 2088-8708

Guided Navigation Control of an Unmanned Ground Vehicle using Global Positioning Systems and Inertial Navigation Systems

Pooja Velaskar, Alvaro Vargas-Clara, Osama Jameel, Sangram Redkar

* Department of Engineering and Computing Systems, Arizona State University, United States

Article Info

Article history:

Received Nov 21, 2013 Revised Mar 3, 2014 Accepted Mar 27, 2014

Keyword:

Unmanned Ground Vehicle Global Positioning System Inertial Navigation System Ardupilot

ABSTRACT

This paper demonstrates the use of Global Positioning System (GPS) and Inertial Navigation System (INS) in order to develop an Unmanned Ground Vehicle (UGV) devised to perform a wide variety of outdoor tasks. There are many applications for autonomous UGVs such as tactical and surveillance applications, exploration of areas inaccessible by humans. Capable to navigate to a specific location, and control their motion depending on their surroundings without human intervention. The inertial navigation system makes use of Inertial Measurement Units (IMUs) to measure the change to the UGV's positional parameters, orientation and speed which are continuously monitored and updated. With the advent of GPS, and the positional data from the inertial system the positional information is computed leading to a more accurate control of the UGV; which otherwise suffers from integration drift that occurs with the implementation of inertial systems alone. Autonomous control of the UGV is implemented by coupling GPS sensor and Mission Planner, a tool to map waypoints from Google Maps. Furthermore, system stability and ideal PID (Proportional, Integral and Derivative) values are determined using bicycle modeling analysis to achieve better estimates and control of the UGV.

Copyright © 2014 Institute of Advanced Engineering and Science.

All rights reserved.

Corresponding Author:

Sangram Redkar,

Department of Engineering and Computing Systems,

Arizona State University,

7001, E. Williams Field Road, Mesa, AZ-85212, United States.

Email: sredkar@asu.edu

1. INTRODUCTION

A UGV most often operates without any on-board operator or human intervention. It is broadly used in tasks where it is almost impossible for a human to be present. Naturally, it finds applications in numerous fields such as military, space exploration, environment sensing, search and rescue. Generally, it is equipped with a controller and on-board sensors to observe the environment and it autonomously makes decisions or pass off the information remotely to an operator through some means of telecommunication. Advances in computer processing techniques, miniaturization, image processing, and communication techniques have resulted in rapid progress in the field of autonomous vehicles. UGVs are now able to sense their world using electro-optic and infrared cameras, and a variety of other sensors. They are able to capture, represent and interpret their environment and autonomously combine and manipulate this information through a series of control actions. Additionally, the prices of the technologies have dropped considerably such that autonomous systems are approximately 80% cheaper than they were in 1990 [1]. Currently, UGVs are deployed for surveillance, mine clearance, firefighting. This research deals with implementing such an autonomous UGV by integrating two different systems, Global Positioning System (GPS) and Inertial Navigation System (INS).

330 ☐ ISSN: 2088-8708

1.1 Global Positioning System:

The Global Positioning System as depicted in Figure 1 is a space-based satellite system that provides positioning, navigation, and timing data to users worldwide and has become a key component in economic growth, transportation safety and critical national infrastructure in the United States and abroad [2]. It operates in all weather conditions, anywhere on or near Earth where there is an unobstructed line of sight to four of more GPS satellites. It is maintained by the United States Government and is freely available to anyone with a GPS receiver. GPS satellites orbit the earth every 12 hours, emitting continuous navigation signals. With the proper equipment, users can receive these signals to calculate time, location and velocity. The signals are so accurate, time can be figured to within a millionth of a second, velocity within a fraction of a mile and location to within 100 meters [3]. Also, the accuracy of the GPS signal in space is actually the same for both the civilian GPS service (SPS) and the military GPS service (PPS). However, SPS broadcasts on only one frequency, while PPS uses two. This means military users can perform ionospheric correction, a technique that reduces radio degradation caused by the Earth's atmosphere. With less degradation, PPS provides better accuracy than the basic SPS [4].

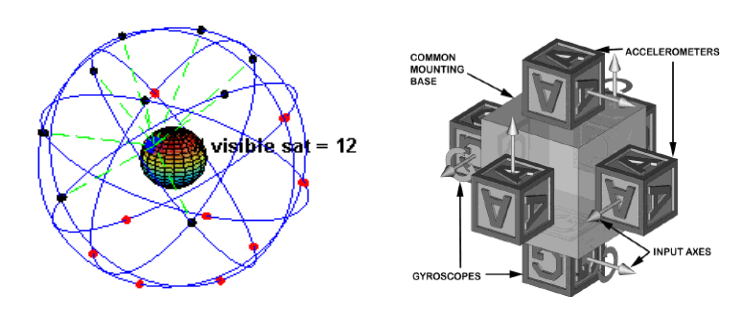


Figure 1. GPS Satellite and constellation (left). Inertial Sensor Assembly (right)

A few of its dominant features have been jotted down below.

- -Extremely accurate, three-dimensional location information (latitude, longitude and altitude), velocity (speed and direction) and precise time.
- -A worldwide common grid that is easily converted to any local grid.
- -All-weather operations
- -Supports unlimited number of users and areas.
- -Supports to civilians at a slightly less accurate level.
- -Continuous real-time operation

1.2 Inertial Navigation System:

An Inertial Navigation System is a navigation tool that uses a controller, motion sensors, rotation sensors to continuously calculate the position, orientation, and velocity of a moving object via a method called dead reckoning. The following is a breakdown of a few terminologies pertaining to INS.

Dead Reckoning- The term, dead reckoning or *deduced* reckoning means the process of estimating the value of any variable quantity by using another quantity and adding to it whatever changes have occurred in the meantime. In navigation, it is the process of calculating one's current position by using a previously determined position, and moving to the new position based upon known or estimated speed over elapsed time, and course. Basically, it relies on knowing where you started from, plus some form of heading information and estimate of speed and time to determine the distance travelled [5].

Inertial Reference frames- These are the non-rotating and non-accelerating coordinate frames in which Newton's laws of motion are valid.

Inertial sensors- These are the sensors that measure inertial accelerations and rotations. *Accelerometers* measure the linear acceleration of the system in the inertial reference frame. They are fixed to the system and rotate with it, unaware of their own orientation. *Gyroscopes* measure the angular velocity of a given system by using its original orientation as the initial condition and integrating the angular velocity.

Inertial Measurement Units (IMUs) – IMUs include *Inertial Sensor Assemblies* as shown in Figure 1, which are a set of inertial sensors mounted on a rigid base, a processor and other support electronics that aid in calibrating and control of the INS.

Figure 2. Loosely coupled GPS-INS (left). Tightly coupled GPS-INS (right)

1.3 GPS-INS Integration

Inertial Navigation Systems have been used for countless navigational operations for the past few decades. Initially, a majority of these systems were very expensive because of costs of high-quality, well-characterized sensors, and the need for a stabilized sensor platform. This high-cost limited their applications to military, scientific, and commercial aircraft. Also, the use of stabilized platforms led to INS having a size and power requirements too large for many applications. Advances in material processing have made it possible to produce small, low-cost inertial sensors [6]. However, inertial systems suffer from a certain phenomenon which is explained as follows.

Integration drift- An INS is initially given position and velocity information from another source, and thereafter it generates its own updated position and velocity by integrating information received from the motion sensors. So, any small errors which arise in the measurement of acceleration and angular velocity are integrated into progressively large errors. This drawback of the INS is called integration drift.

As these low-cost sensors cannot be expected to meet the accuracy and precision requirements of many navigation applications. Therefore, with GPS capability for on-line calibration and error estimation, it is used along with INS. Now, among the most detrimental factors affecting a GPS based vehicular navigation system is the obstruction of the line of sight between vehicle and satellites. As users travel in urban canyons and high foliage areas, the ability of GPS to provide an accurate position is compromised. Although high sensitivity GPS (HSGPS) receivers can track weak signals through fading effects, this makes them susceptible to multipath which is the phenomenon of radio signals reaching the antenna via two or more paths causing signal jamming [7]. Here, INS can act as a short-term fall-back when GPS signals are unavailable. Thus, as GPS and INS have complementary characteristics, their implementation is considered in an integrated approach.

Sensor technology made headway with the inventions such as stand-alone gyrocompasses (1930), Schuler tuned "Floated rate integrating gyro developed by MIT, USA (1950), dynamically tuned gyro (1960), fiber optic gyro etc. Moreover, GPS was introduced at the end of the 20th century [8]. Research proved that GPS and INS shortcomings were nullified with their integration. GPS-INS architectures were developed mainly as loosely and tightly coupled systems, as illustrated in Figure 2. Their working is briefly depicted in the block diagrams.

The traditional approach to INS/GPS integration with Kalman filters leads to a configuration termed 'loosely coupled', shown in Figure 2. In this structure a GPS filter (generally EKF or Least-squares recursion) processes the GPS signals and outputs three dimensional position (and possibly velocity) in the standard GPS Earth Centered Earth Fixed (ECEF) reference frame. The design of the GPS system requires four satellites to be tracked in order to solve for three dimensional position (a fourth time uncertainty is also solved). When less than four satellites are visible, stand-alone three dimensional GPS positioning cannot be accomplished. Loosely coupled configurations employ a second, master Kalman Filter to predict inertial sensor errors from the equations of inertial navigation. The filter is updated with direct observations of the position error formed from the outputs of the inertial unit and the GPS filter. The standard Kalman filter equations are optimal when sensor observations are unbiased with white noise. By filtering the GPS data twice this optimality constraint is effectively abandoned [9]. GPS ranging signals are fused directly in the update stage of the Kalman filter. The more satellites used in the ranging process the more information the filter has to constrain the inertial navigation solution.

In a situation of degraded GPS availability, a 'tightly coupled' configuration is capable of updating the filter with only one visible satellite. This configuration is illustrated in Figure 2. In addition, a tightly coupled filter processes the GPS signals directly. In a well designed system this increases the chance of optimal filter performance [9]. Kalman Filter Smoothening algorithm was developed to post process the data to obtain position solution when not directly available.

Research regarding this work is discussed below. In 2006, Godha discussed the use of MEMS IMUs for vehicular navigation, including the use of height and non-holonomic velocity constraints. Other research in the same area includes: Salychev et al. (2000), Mathur and Grass (2000), Kealy et al. (2001). McMillan incorporated two IMUs in a Kalman filter for marine applications. The system, called Dual Inertial Navigation System (DINS) used a reference system to test other navigation systems, e.g. Scherzinger et al. (1996 & 1997). While it provided fault detection on IMU measurements, its main focus was to provide redundancy in case of single IMU failure. Brand and Philips (2003) introduced the use of two IMUs for pedestrian navigation using MEMS IMUs. Their method used additional RF observables to directly observe the distance between IMUs. Petovello et al. (2005) used a dual GPS/INS methodology to quantify ship flexure in aircraft carriers. Two sets of INS were used to determine the relative position of each inertial system and each INS was provided GPS observables through the use of a GPS antenna and receiver [7]. Randle and Horton described in their works the integration of GPS/INS using a low cost IMU consisting of micro-machined sensors and on-board calibration. Simulations have been done for both flight and automotive navigation. Thus, the research on GPS-INS integration continues to focus on achieving high performance positioning for growing applications and areas.

1.4 Description and Scope:

This research is divided into two parts, i) Building a UGV (named Ardurover as it is built using Ardupilot Mega) with integrated GPS and INS and ii) Bicycle model analysis. The practical aspect of this research limits itself to the operation of the Ardurover in manual mode and following three different waypoint courses in auto mode. While the theory aspect deals with the development of a bicycle model using the parameters of the implemented Ardurover to generate a set of PID values for optimum control of the UGV.

2. RESEARCH METHOD

This part of the work deals with modeling the vehicle to study the path tracking and stability of motion of the UGV to navigate freely in unknown environments. The modeling technique used here, is the three degree-of-freedom *bicycle modeling*, which is a common approximation used for motion planning, simple vehicle analysis and deriving intuitive control algorithm. This is done by the assumption of combining the left and right side of the wheel of a car into a single in-line pair of wheels. The path-tracking control of an autonomous vehicle is one of the most difficult automation challenges because of constraints on mobility, speed of motion, undulating terrain etc. The vehicle control can be separated into lateral and longitudinal controls. Here, we focus on the lateral control to follow a trajectory in terms of heading and path control.

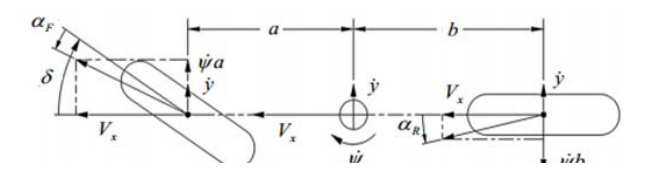


Figure 3. Bicycle Model [10]

Bicycle Model

This simple bicycle model can be used to derive control laws (equations of motion) by assuming the four-wheeled vehicle as a two-wheeled bicycle model. The two degrees of freedom are lateral (vehicle fixed y) and yaw (heading). The external forces and torques acting on the vehicle are two main types: tire contact forces and aerodynamic forces. The vehicle motion dealt in this project is mainly generated by the tire forces alone assuming that aerodynamic forces acting on a city road are minimal. Three forces act upon the tire, namely longitudinal force, lateral force and vertical force. The effect of the longitudinal force causes vehicle traction and braking. The effect of the vertical force is good adhesion of the vehicle to the road [8]. The effect of the lateral force is to make the vehicle turn as well as push it sideways. This project deals with only this lateral force. The wheels of the vehicle are affected by the slip angle at the tires. The slip angle for an individual tire is defined as the direction that the wheel is pointing to the direction that the center of the wheel is moving. Slip angles conform to the sign conventions defined for the body fixed coordinate system; clockwise rotation is defined as positive. A positive steering angle produces at a right turn, but slip angles are

negative [10]. To linearize the system, we assume that the vehicle is disturbed merely by the small perturbation in the equilibrium point, that is, small angle approximation is used. Figure 3 shows the bicycle model showing velocities at the tires for a right turn with negative slip angles. The important variables are: δ is steering angle (Positive CW in top view), V_x is forward (longitudinal) speed, α_F is front tire slip angle, α_R is rear tire slip angle, α is distance from CG (Center of gravity) to front axle, δ is distance from CG (Center of gravity) to rear axle, δ is lateral speed (positive up), and $\dot{\Psi}$ is yawing speed (positive CW in top view).

A. Dynamical Equations of motion for lateral and yaw dynamics:

From the above figure, the front and rear slip angles are represented in the following equations:

$$\alpha_F = \tan^{-1} \left(\frac{\dot{y} + \dot{\Psi}a}{V_x} \right) - \delta \cong \frac{\dot{y}}{V_x} + \frac{\dot{\Psi}a}{V_x} - \delta, \alpha_R = \tan^{-1} \left(\frac{\dot{y} - \dot{\Psi}b}{V_x} \right) \cong \frac{\dot{y}}{V_x} - \frac{\dot{\Psi}b}{V_x}$$
 (1)

A linear constitutive equation is used for the tires to calculate the lateral force generated by the tires as a function of slip angle. The corresponding forces are the tire cornering stiffnesses multiplied by the slip angle.

$$F_{yF} = -C_F \alpha_F = -C_F * \frac{\dot{y}}{V_x} - C_F * \frac{\dot{\Psi}a}{V_x} + C_F \delta, F_{yR} = -C_R \alpha_R = -C_R * \frac{\dot{y}}{V_x} + C_R * \frac{\dot{\Psi}b}{V_x}$$
 (2)

Where, C_F = Front tire cornering stiffness (always positive)

 C_R = Rear tire cornering stiffness (always positive)

The total lateral acceleration is the centripetal acceleration plus the direct lateral acceleration (ÿ), as given below.

$$a_{y} = \ddot{y} + V_{x}\dot{\Psi} \tag{3}$$

Expressing the centripetal acceleration as $V_x\dot{\Psi}$ produces the correct sign (direction) for the centripetal acceleration.

Applying Newton's 2nd law yields:

$$\left(\ddot{y} + V_x \dot{\Psi}\right) m = F_F + F_R = -C_F \frac{\dot{y}}{V_x} - C_F \frac{\dot{\Psi}a}{V_x} + C_F \delta - C_R \frac{\dot{y}}{V_x} + C_R \frac{\dot{\Psi}b}{V_x}$$

$$\tag{4}$$

The tire forces also produce a moment acting on the vehicle and application of the angular momentum principle yields:

$$I_{\varepsilon}\ddot{\Psi} = F_{F}a - F_{R}b = -C_{F}a\frac{\dot{y}}{V_{\varepsilon}} - C_{F}\frac{\dot{\Psi}a^{2}}{V_{\varepsilon}} + C_{F}a\delta + C_{R}b\frac{\dot{y}}{V_{\varepsilon}} - C_{R}\frac{\dot{\Psi}b^{2}}{V_{\varepsilon}}$$

$$(5)$$

Rearranging equations (4) and (5), we get the final dynamic equations governing lateral and yaw motion:

$$\ddot{y} = -\dot{y} \left(\frac{C_F + C_R}{mV_X} \right) - \dot{\Psi} \left(\frac{C_F a - C_R b}{mV_X} - V_X \right) + \frac{C_F \delta}{m} \tag{6}$$

$$\ddot{\Psi} = -\dot{y} \left(\frac{C_{F}a - C_{R}b}{I_{E}V_{x}} \right) - \dot{\Psi} \left(\frac{C_{F}a^{2} + C_{R}b^{2}}{I_{E}V_{x}} \right) + \frac{C_{F}a\delta}{I_{E}}$$
(7)

B. Parameter Identification for UGV:

The above differential equations can be used to model any vehicle after choosing appropriate parameters. Some parameters can be directly measured or calculated and some have to be estimated using

known information. The accuracy of such parameters is likely low. The following are the parameters, their SI units, and their corresponding method of measurement/estimation.

- 1. m (Mass of the Vehicle)- Directly measured in kilograms.
- 2. a (Distance from CG to front axle)- Directly measured in meters
- 3. b (Distance from CG to rear axle)- Directly measured in meters
- 4. V_x (Longitudinal velocity)- The set velocity of Ardurover in m/sec
- 5. C_F (Front tire cornering stiffness) & C_R (Rear tire cornering stiffness)- Estimated based on available data on RC car JAC 2164 Pink Sedan [11].
- 6. I_{ϵ} (Yaw moment of Inertia)- The Ardurover was treated as a rectangular box and its length and width were measured. The moment of inertia was found out by the formula:

$$I_z = m \left(\frac{w^2 + l^2}{12} \right)$$

The values for the above parameters for UGV are found out to be:

m = 0.927 kg, a = 0.2032 m, b = 0.1524 m, $V_x = 1 \text{m/s}$, 3 m/s, 6 m/s, 10 m/s

$$C_F = 30.2 \text{ N/rad}, C_R = 21.0 \text{ N/rad}, I_z = 0.1221 \text{ kg*m}^2$$

Heading control:

For heading control, the objective is to move along a desired heading. The control variable is steering and output variable is heading (yaw), which is controlled to steer toward a waypoint. Equations (6) and (7) can be written in terms of constants such as:

$$\ddot{y} = -\dot{y}A - \dot{\Psi}B + \delta C, \quad \Psi = -\dot{y}D - \dot{\Psi}E + \delta F \tag{8}$$

Where the constants are defined by:

$$A = \frac{C_F + C_R}{mV_x}, B = \frac{C_F a - C_R b}{mV_x} - V_x, C = \frac{C_F}{m}, D = \frac{C_F a - C_R b}{I_z V_x}, E = \frac{C_F a^2 + C_R b^2}{I_z V_x}$$
$$F = \frac{C_F a}{I_z}$$

Taking the Laplace transform and solving for the open loop transfer function from steering angle (δ) to heading angle $(\dot{\Psi})$ yields:

$$\frac{\Psi(s)}{\delta(s)} = \frac{Fs + FA - CD}{s^3 + s^2(A+E) + s(AE - BD)} \tag{9}$$

A PID control logic is employed:

$$\frac{\delta(s)}{e(s)} = K_p + \frac{K_I}{s} + K_D s \tag{10}$$

Where e(s) is the error between the heading (Ψ) and the desired heading (Ψ_d). The corresponding closed transfer function simplified using Maple is:

$$\frac{\Psi(s)}{\Psi_{d}(s)} = \frac{FK_{D}s^{3} + s^{2}(AFK_{D} - CDK_{D} + FK_{p}) + s(AFK_{p} - CDK_{p} + FK_{t}) + AFK_{t} - CDK_{t}}{s^{4} + s^{3}(FK_{D} + A + E) + s^{2}(AFK_{D} + K_{p}F + AE - CDK_{D} - BD) + s(AFK_{p} + AFK_{t} - CDK_{p}) + AFK_{t} - CDK_{t}}$$
(11)

A. 3D plot for stable values of Kp, Ki, Kd:

Equation (11) is substituted with values of A, B, C, D, E, F and not the values of Kp, Ki and Kd. The resulting equation's characteristic equation is used to find stable values for Kp, Ki and Kd. The characteristic equation for the closed-loop transfer function is found out to be:

 $s^4+s^3(502.59Kd+197.30)+s^2(19924.73Kd+502.59Kp+7325.71)+s(2775.08Ki+19924.7Kp)+19924.73Ki=0$

The values of A,B,C,D,E,F and Kp, Ki, Kd (used for Ardurover) are substituted in the above equation and using MATLAB, the root loci are plotted for $V_x = 1 \text{ m/s}$, 5 m/s and 10 m/s.

B. Resulting plots for heading control:

This section depicts the outcome of the heading control bicycle modeling analysis in terms of graphing stable Kp, Ki, Kd values and root locus plots.

1. 3D Surface plots for stable PID values:

The following are the 3D surface plots for PID values for ranges $V_x = 1$ m/s and 3 m/s

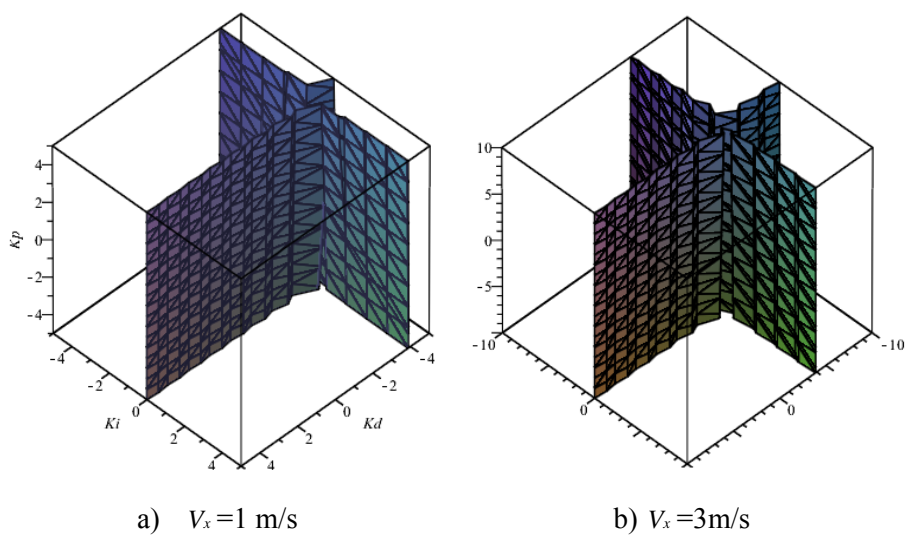


Figure 4. Kp, Ki, and Kd for ranges -5 to 5 (for $V_x = 1 \text{ m/s}$), and for ranges -10 to 10 ($V_x = 3 \text{ m/s}$)

2. Root locus:

The following are the digital root loci plot for varying velocities and Kp, Ki, Kd set as 0.900, 0.020 and 0.040 respectively.

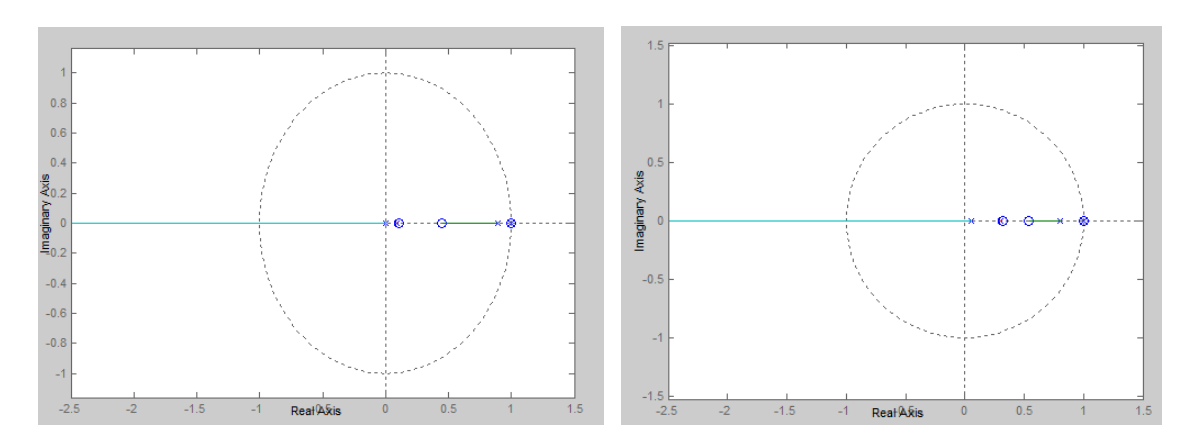


Figure 5. Root locus of heading control for $V_x = 1 \text{m/s}$ (left), and $V_x = 3 \text{ m/s}$ (right).

336 □ ISSN: 2088-8708

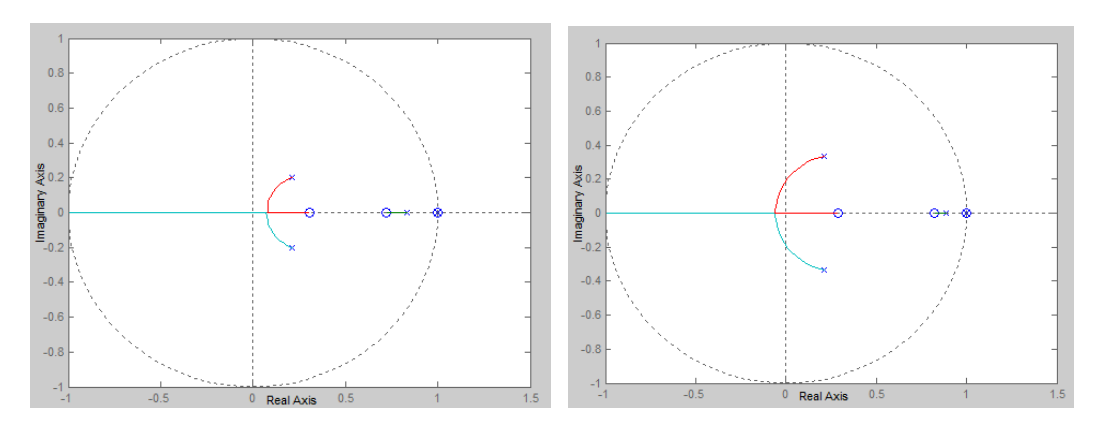


Figure 6. Root locus of Heading control for $V_x = 6$ m/s (left), and $V_x = 10$ m/s (right)

The root loci are obtained by varying proportional gain Kp. When the gain is small, the poles start at the poles of the transfer function and as gain becomes higher, poles and zero tend to overlap. Each locus starts at a pole and ends at a zero. Here, as roots lie on the unit circle, the system is marginally stable. In cases where some of the loci end at zero located infinitely far from poles. This happens when the system has more poles than zeros.

Path control:

Path control is another control approach that is useful in minimizing the lateral displacement of the vehicle from the straight line path between two waypoints. To comply with a Linear Time Invariant (LTI) system, a few changes are made. The straight path between waypoints has a global heading angle. The path is rotated by this angle to that it is parallel with the earth-fixed X-axis. It is then translated so that the previous waypoint is at origin. Thus, the earth-fixed Y displacement is the path error. To linearize the system, the heading angle is assumed to be small. Now, integrating equation (7) yields heading (Ψ). Using this heading angle, the linear velocities are transformed into the earth fixed coordinate system. The kinematic coordinate transformations are:

$$\dot{\mathbf{X}}_{\text{earth}} = V_x \cos(\Psi) - \dot{\mathbf{y}} \sin(\Psi) \tag{12}$$

$$\dot{Y}_{\text{earth}} = V_{x \sin}(\Psi) + \dot{y} \cos(\Psi) \tag{13}$$

If Ψ is assumed to be small, then equation (13) reduces to the following equation, where \dot{y} is the lateral velocity and V_x is the longitudinal velocity.

$$\dot{Y}_{earth} = V_x \Psi + \dot{y} = \dot{e} \tag{14}$$

The open loop transfer function uses steering angle as an input and the perpendicular displacement in the Y_{earth} direction, and (e) as an output. Thus, a relationship between lateral displacement (y) and steering angle (δ) is needed to make Equation (14) into the required transfer function. The transfer function between vaw and steering angle was found in Equation (9) and is rewritten here.

$$\Psi(s) = \frac{Fs + FA - CD}{s^3 + s^2(A+E) + s(AE - BD)} \delta(s)$$
(15)

Similarly, the transfer function between lateral displacement and steering angle is found out by solving equations (8) for lateral displacement instead of yaw angle and is,

$$y(s) = \frac{Cs + CE - BF}{s^3 + s^2(A+E) + s(EA - BD)} \delta(s)$$
(16)

The Laplace transform of equation (14) contains both $\Psi(s)$ and y(s):

$$s Y_{earth}(s) = V_x \Psi(s) + sy(s)$$
(17)

Solving equations (15-17) for the transfer function $\frac{Y_{\text{earth}}(s)}{\delta(s)}$ yields:

$$\frac{Y_{\text{earth}}(s)}{\delta(s)} = \frac{s^2C + s(V_xF + CE - BF) + V_x(FA - CD)}{s^4 + s^3(A + E) + s^2(EA - BD)}$$

$$(18)$$

The closed-loop function when combined with a PID controller yields the following equation:

$$\frac{Y_{\text{earth}}(s)}{\delta(s)} = \frac{CK_D s^4 + s^3 (Kd(-BF + CE + FV_x) + CK_p) + s^2 (K_p(-BF + CE + FV_x) + CK_I + K_D(AFV_x - CDV_x + C)) + ...}{s^5 + s^4 (A + E + AE + CK_D) + s^3 (CK_p + K_D(-BF + CE + FV_x) + AE - BD) + ...}$$

$$\frac{... + s(K_p(AFV_x - CDV_x) + K_I(-BF - CE + FV_x)) + K_IV_x(AF - CD)}{... + s^2 (K_p(-BF + CE + FV_x) + CK_I + K_D(AFV_x - CDV_x)) + s(K_p(AFV_x - CD) + K_I(-BF + CE + FV_x) + K_IV_x(AF - CD)}{... + s^2 (K_p(-BF + CE + FV_x) + CK_I + K_D(AFV_x - CDV_x)) + s(K_p(AFV_x - CD) + K_I(-BF + CE + FV_x) + K_IV_x(AF - CD))}$$
(19)

Using the above closed loop transfer function, parts 1 and 2 described in heading control are repeated to plot the 3D plot of stable values of Kp, Ki, Kd and root locus for stability analysis.

A. Resulting plots for Path control:

1. 3D Surface plots for stable PID values:

The following are the 3D surface plots of stable PID values for $V_x = 1$ m/s and $V_x = 3$ m/s

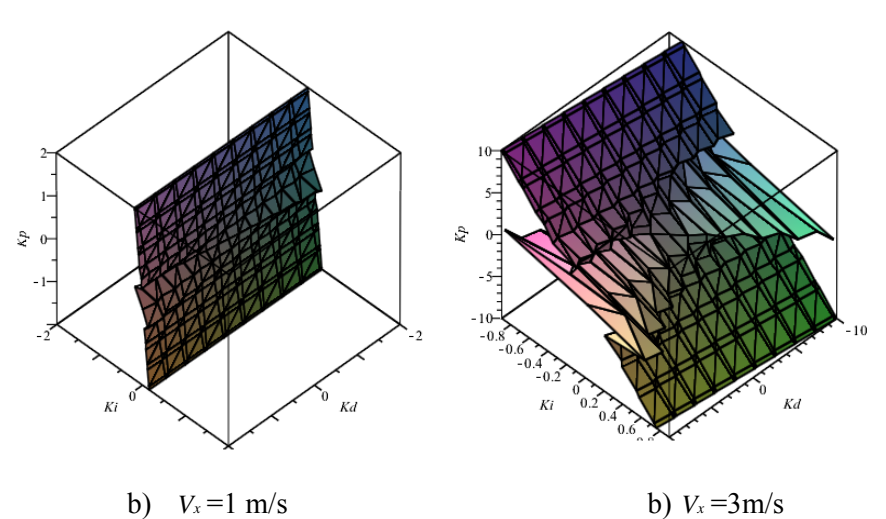


Figure 7. Kp, Ki, and Kd for $V_x = 1$ m/s, and Kp, Kd and Ki for $V_x = 3$ m/s

Root locus:

The following are the analog root loci plot for varying velocities and Kp, Ki, Kd set as 0.900, 0.020 and 0.040 respectively.

338 □ ISSN: 2088-8708

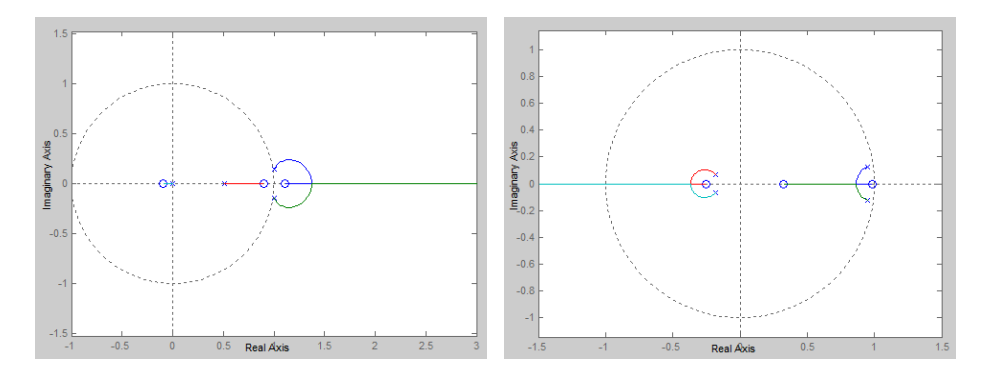


Figure 8. Root locus of path control for $V_x = 1$ m/s (left), and $V_x = 3$ m/s (right)

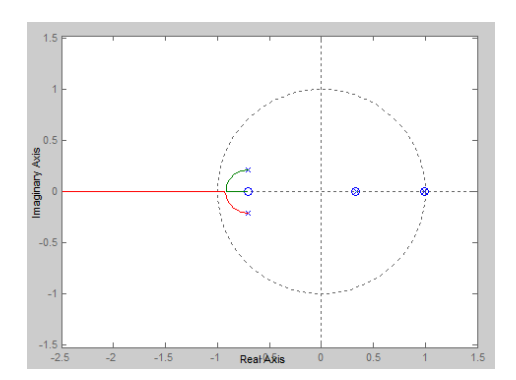


Figure 9. Root locus of path control for $V_x = 6 \text{ m/s}$

For, $V_x = 1$ m/s, the system is highly unstable as the poles lie outside the unit circle. For, $V_x = 3$ m/s, all poles lie inside the unit circle rendering the system stable. The system with $V_x = 6$ m/s is marginally stable.

The vehicle being modeled and analyzed for the various PID parameters and velocities, the Ardurover was put into action.

3. RESULTS AND ANALYSIS

The Ardurover was tested in an empty lot in ASU's Polytechnic campus. Figure 10 depicts the Ardurover set up and the missions were conducted on concrete lots. Figure 10 shows the UGV connected to the ground station wirelessly through telemetry.

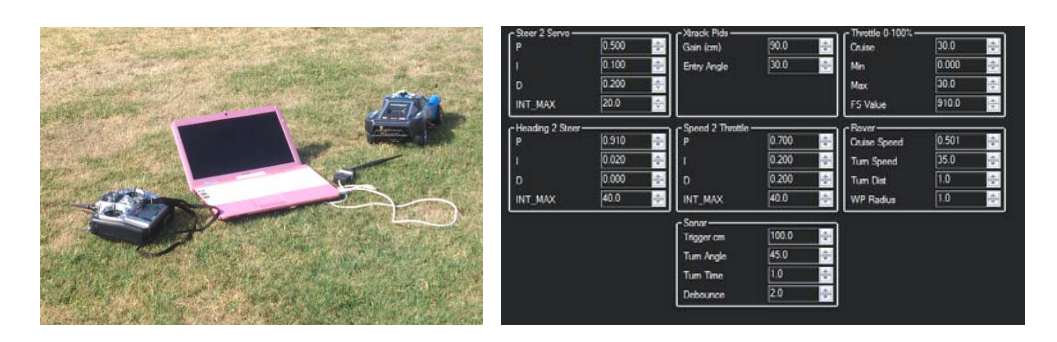


Figure 10. Ardurover setup on field (left), and PID parameters (right)

After powering on the Ardurover and the transmitter, Mavlink communication was established using the 'Connect' button. Before starting a mission, PID tuning had to be done to ensure reliable navigation and performance in the wind.

The Proportional gain (P) is the simplest form of control. It is the "present" error. Past data ("I") is taking into consideration recent error. If Proportional gain cannot drive the control surface to zero the error, then "I" gain will attempt to do so. Future ("D") is extrapolation of the current error into the future for some period. We choose a control input to attempt to head off the predicted (future) change. The PID parameters that were selected are shown in Figure 10. To check the performace of controller two desired trajectories were programmed (as shown in yellow in Figure 11 and 13). Figure 11 is a simple circular track where the vehicle (shown in purple) is programmed to follow a circular path (indicated by green waypoints and yellow line). The actual path followed by the vehicle is shown in blue. For the initial attempt (shown in figure 11) it can be noted that the vehicle drifted between waypoint five and six as GPS was unavailable for a brief period of time. However, the vehicle corrected itself once the GPS lock was obtained again.



Figure 11. Waypoint trajectory 1

In order to improve the performance the D value in the controller was lowered and the test was repeated as shown in figure 12. It can be noted that the vehicle (shown in purple) tracked the desired path better. The RMS error between the desired and actual path for initial test (shown in figure 11) was 2.31 m and the RMS error for second test (shown in Figure 12) was 1.64 m.



Figure 12. Waypoint trajectory 2

340 □ ISSN: 2088-8708

In second course; a straight line path was programmed. During the test with the same controller gains the vehicle exhibited an offset and turned before the waypoint 4 was actually reached.



Figure 13. Waypoint trajectory 3

After performing the tests, onboard data was downloaded and analyzed. The logs contain information such as mode, GPS latitudes and latitudes, attitude information such as roll, pitch and yaw.



Figure 14. Log information during Auto mode

Telemetry log was also used to play back missions as shown Figure 15.

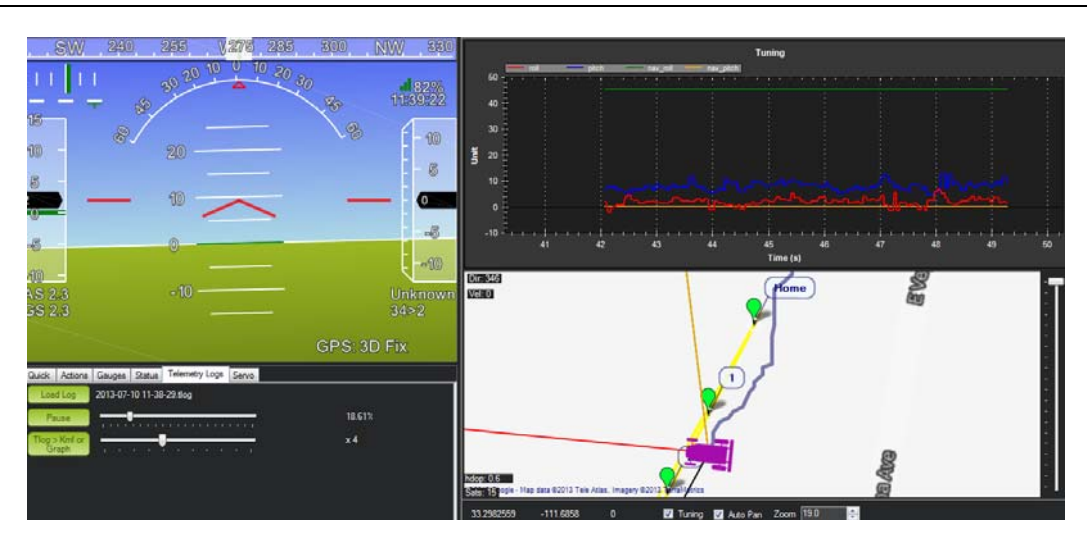


Figure 15. Replaying telemetry log

The telemetry log was obtained wirelessly via zigbee network and can be used to replay the mission and investigate the controller performance.

4. CONCLUSION

This project presented the manual and autonomous behavior of the UGV using GPS and INS along with its modeling. There are numerous ways in which the performance of the rover can be enhanced. A better GPS receiver like the u-blox receiver can greatly reduce the GPS reported heading leading to improved heading control. It is able to provide an accurate reference frequency to within 1 part in 100 billion. PID tuning needs to be perfected for accurate waypoint following. As observed in testing PID gains for the circular path may not be the best when the veicle is travelling in a straight line. Thus an adaptive PID controller may be useful to improve performance. Adaptive PID control can help the system to adapt to external environments and complexity of vehicle dynamics

The bicycle model can be improved if the corner stiffnesses of car tires were actually measured than estimated from the scaled down data of actual car tires. The yaw moment of inertia was calculated by assuming the UGV as a reactangle, which was actually not the case. The size and position of the autopilot circuitry and battery should also be accounted when computing moment of inertia. The analysis could also be enhanced for variations in mass, center of gravities and vehicle geometry.

Currently the UGV is being improved using a high update rate GPS receiver, more powerful processor and an adaptive Brain Emotional Learning Based Controller (BELBIC). These improvements are expected to improve the performance of UGV and the results will be published leter.

REFERENCES

- [1] Anthony Finn, Steve Scheding, "Developments and challenges for autonomous unmanned vehicles", Heidelberg, Springer, Berlin, 2010, pp.11
- [2] United States Government Accountability Office, "Global Positioning System-Challenges in Sustaining and Upgrading Capabilities Persist", Washington, D.C, pp. 1, September, 2009
- [3] United States, Department of the Air Force, "Global Positioning System", U.S Air Force Fact Sheet, Washington D.C, March 2007
- [4] GPS. gov. "Official U.S. Government information about the Global Positioning System (GPS) and related topics". NOAA, n.d. Web. <ww.gps.gov>.
- [5] Mohinder S. Grewal, Angus P. Andrews, Chris Bartone, "Global navigation satellite systems, inertial navigation, and integration", John Wiley & Sons, 3rd Edition, Hoboken, New Jersey, 2013, pp.3
- [6] Jay A. Farrell and Matthew Barth, "The Global Positioning System and Inertial Navigation", McGraw Hill, New York, 1998
- [7] Jared B. Bancroft, "Multiple IMU Integration for Vehicular Navigation", Session D2, Savannah, GA, 22-25 September, 2009
- [8] Ipsit Dash, "Effectiveness of INS and GPS Integration from an Urban perspective", AH2916, 2013
- [9] Michael George, Salah Sukkarieh, "Tightly Coupled INS/GPS with Bias Estimation for UAV Applications", Centre for Autonomous Systems, University of Sydney, Australia, n.d.

[10] James Patrick Massey, "Control and waypoint navigation of an autonomous ground vehicle", Texas A&M University, May 2006

[11] Midshipman Philip C. Hoblet, "Scale-model vehicle analysis for the design of a steering controller", U.S.N.A-Trident Scholar project report no. 309, United States Naval Academy, Maryland, 2003

BIOGRAPHIES OF AUTHORS



Pooja Velaskar graduated from Arizona State University with MS (Tech) in Fall-2013. Her interests are in the area of inertial navigation, GPS and Vehicle dynamics.



Alvaro Vargas-Clara is a PhD student at Arizona State University. He is pursuing PhD in the Simulation Modeling and Applied Cognitive Science program. His research interests are in the area of dynamics, control and navigation.



Osama Jameel graduated from Arizona State University with MS (Tech) in Fall-2013. His interests are in the area of dynamics and control. He is currently working as an instrument shop supervisor at Department of Engineering and Computer Systems and College of Technology and Innovation.



Sangram Redkar is an Associate Professor at Department of Engineering and Computer Systems and College of Technology and Innovation. His research interest are dynamics, control and machine design